Insights into the electrocatalytic behavior of nitrogen and sulfur co-doped carbon nanotubes toward oxygen reduction reaction in alkaline media

Gutru Rambabu, Zarina Turtayeva, Feina Xu, Gaël Maranzana, Mélanie Emo, Sebastien Hupont, Mohamed Mamlouk, Alexandre Desforges, B. Vigolo

J Mater Sci (2022) 57:16739–16754

Energy materials

Insights into the electrocatalytic behavior of nitrogen and sulfur co-doped carbon nanotubes toward oxygen reduction reaction in alkaline media

Gutru Rambabu[1,2,3,*], Zarina Turtayeva[2], Feina Xu[2], Gael Maranzana[2], Mélanie Emo[1], Sébastien Hupont[1], Mohamed Mamlouk[3], Alexandre Desforges[1], and Brigitte Vigolo[1]

[1] Université de Lorraine, CNRS, Institut Jean Lamour, 54000 Nancy, France
[2] Université de Lorraine, CNRS, LEMTA, 54000 Nancy, France
[3] School of Engineering, Newcastle University, Newcastle Upon Tyne, UK

Received: 12 April 2022
Accepted: 16 August 2022
Published online: 4 September 2022

ABSTRACT

This study examines the effect of pretreatment and doping to enhance the ORR activity of multiwalled carbon nanotubes (MWCNTs). Melamine and thio-urea are chosen as precursors for mono and co-doping, respectively. A series of samples with pristine and pretreated CNTs are prepared and characterized physicochemically by Raman spectroscopy, X-ray photoelectron spectroscopy (XPS) and transmission electron microscopy (TEM) and electrochemically by cyclic voltammetry (CV) and linear sweep voltammetry (LSV). The obtained results show that co-doping is an effective way for improving ORR activity, due to the synergistic effect of N and S for changing the charge and spin density, respectively. Moreover, thio-urea favors the proportion of pyridinic and graphitic nitrogen configurations within doped samples. As a consequence, our synthesis method gives samples with superior ORR activity. The maximum ORR activity is obtained for NS-OX-CNTs which shows an over potential of 0.95 V vs RHE at 0.1 mA/cm^2, which is comparable to Pt/C (0.98 V vs RHE). The electron transfer number (n) is calculated as 3.9 at 0.4 V which suggests that the ORR proceeds through a dominant 4 e$^-$ path. These comparable half-cell results to that of Pt/C pave the way for further testing as cathode materials for anion exchange membrane fuel cells (AEMFC).

Handling Editor: Kyle Brinkman.

Address correspondence to E-mail: rambabu.gutru@newcastle.ac.uk

https://doi.org/10.1007/s10853-022-07653-3

GRAPHICAL ABSTRACT

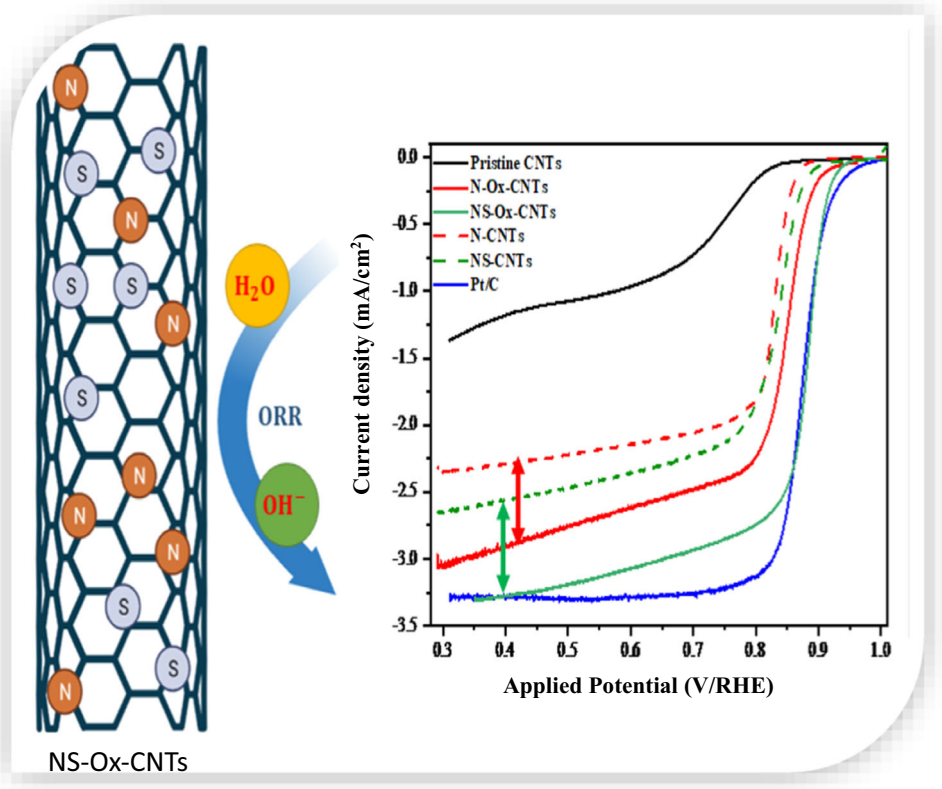

Introduction

In contrast to the acidic medium, a lot of catalyst materials can be used under basic medium with high efficiency such as non-precious metal catalysts or metal-free catalysts [1]. For instance, oxygen reduction reaction (ORR) is known as a key reaction for many electrochemical devices such as fuel cells and metal–air batteries [2]. In acidic medium, ORR is sluggish and requires noble catalysts like Pt to occur [3]. However, ORR has a lower overpotential in alkaline medium than in acidic medium, which allows the use of Pt-free catalysts [4]. This interest has led significant development in the catalysis research focusing on non-precious metal catalysts and metal-free catalysts.

Over the past decade, significant progress has been observed in the development of non-precious metal catalysts and metal-free catalysts for ORR due to their low cost and enhanced stability [5]. Although some Co (cobalt)- and Fe (iron)-based catalysts have shown remarkable ORR activity in AEMFC, they often suffer from dissolution and/or agglomeration during fuel cell operation, limiting thus further development in fuel cell technology [6]. These limitations have driven to the development of carbon nanomaterial-based catalysts which have good thermal, mechanical and catalytic properties. MWCNTs, with abundant free flowing electrons, are particularly suitable as ORR catalysts [7]. However, these electrically neutral sp^2 carbons reduce the oxygen via 2e- path producing peroxide intermediates [8]. This is why modifying the electronic structure of MWCNT framework by chemical treatment is required to favor its ORR activity [9]. Till date, heteroatom doping is suggested as the best modification strategy for MWCNTs. Electronegative atoms like N, S, B are identified as

potential candidates to dope in sp^2 carbon framework due to their similarity in atomic size with carbon. Nitrogen has higher electronegativity (3.04) than carbon (2.55), and the substitution of N in the carbon framework could induce the change in charge distribution of neighboring carbon atoms [10]. Hence, the carbon atoms adjacent to the inserted N atom are the active sites for ORR in nitrogen-doped carbon nanotubes (N-CNTs). On the other hand, sulfur-doping (S-doping) is also an effective way to increase the ORR activity of carbon materials [11]. Unlike nitrogen, sulfur has an electronegativity almost similar to that of carbon, and hence, its influence on the charge density of carbon is insignificant after doping [12]. But S-doping can alter the spin density of CNT framework and thus creates active sites for the chemisorption of O_2 [13]. That is why breaking the electrical neutrality of carbon framework and creating charged sites for the possible adsorption of oxygen molecules is a key factor to promote ORR activity on carbon-based metal-free catalysts. N-doping, S-doping and NS co-doping are largely explored in graphene-based materials and studied for their ORR activity [14]. Although N-doped CNTs were sufficiently explored, the simultaneous N and S doping (or co-doping with one precursor) is less explored due to the lack of synthesis methods. Two synthesis strategies are mainly adopted to fabricate heteroatom-doped carbon structures, namely in situ and ex situ methods [15]. I*n situ* methods involve the mixing of heteroatom precursors during the growth of carbon structures (CNTs or graphene). On the other hand, ex situ fabrication consists of a thermal annealing of carbon support in the presence of heteroatom precursors. Among the two methods, ex situ method is generally more convenient because the synthesis conditions can be precisely controlled. In fact, some metallic compounds are needed during the in situ growth of carbon synthesis and their presence can lead some misunderstanding of ORR activity results.

Among all the doping strategies, N-doping is the most studied. It is well known that the insertion of nitrogen within CNTs leads different C-N configurations in the honeycomb network, namely pyrolic, pyridinic and graphitic nitrogen. Pyridinic and graphitic N are suggested to enhance the ORR activity [16]. The ORR activity of doped CNTs depends not only on the type of dopant but also on the dopant concentration. Zhu Chen et al. prepared N-doped CNTs (N-CNTs) from chemical vapor deposition of pyridine or ethylene diamine (EDA) in the presence of ferrocene [17]. The prepared N-CNTs with EDA showed higher nitrogen content (5.18%) than the sample prepared with pyridine as solvent (3.41%). Moreover, the ORR activity of the former was higher than the latter and was comparable to Pt/C in alkaline electrolyte. Since both samples were prepared in the presence of ferrocene, they both contained 1% trace amounts of iron. It is interesting to ask whether iron impurities contribute to the ORR activity or whether the results presented are solely due to the contribution of N-doping. On the other hand, ex situ fabrication of N-CNTs via thermal annealing of nitrogen source molecules can also give different amount of nitrogen after doping step [18]. For instance, when melamine and urea are used for CNTs doping, the amount of nitrogen is of 4.8 vs 0.8, respectively, for melamine and urea [19]. The ORR results in alkaline medium indicated that melamine sourced N-CNTs is more active with increased durability.

However, multi heteroatom doping can also be an effective strategy to enhance the ORR activity of CNTs. In the literature, CNT-co-doping has been studied as possible metal-free catalysts for ORR in alkaline media, such as NF, NS and NB-co-doping [7, 20, 21]. In fact, co-doping allows to bring some synergy between the introduced elements and carbon backbone. In the case of NS-co-doping for instance, the insertion of N can impact on the charge density, whereas the presence of S can alter the electronic structure [22]. The combination of the both elements can favor the catalytic activity of the obtained carbon material. However, the co-doping may be carried out with the use of several precursors [8] or a unique precursor containing several desired elements. So, an optimization has to be found like for N-doping.

In this work, we have attempted to apprehend the single and co-doping within MWCNTs as well as its impact on ORR activity. We have examined N-doping and NS-co-doping within MWCNTs. The NS-co-doping was carried out with a single precursor containing the both desired elements. One of the purposes is to check and validate the new strategy of doping, which can tune the electrical and structural properties of CNTs in order to maximize the electrocatalytic activity of nanocarbons through a possible mentioned synergistic effect. In addition, we were interested in the cleaning step of carbon nanotubes

before doping, such as the acid treatment step. This step is often overlooked in the previous reported literature. Such pretreatment can be important since it could strongly impact the doping rate and consequently the electrochemical activity. Eventually, this study would provide a clear guideline for the upcoming studies in this field.

Experimental section

Materials

MWCNTs with an average diameter of 9.5 nm and a length of 1.5 μm were purchased from Nanocyl S.A. (Belgium). Melamine (N source) and thio-urea (N and S sources) with 99% of purity as well as sulfuric acid and nitric acid were procured from ACROS Organics. 1 M NaOH solution under ACS reagent grade was purchased from Aldrich and used as received. Pt/C (40 wt.% of Pt) catalyst powder was purchased from Alfa Aesear for ORR comparison. Nafion ionomer 20 wt.% was procured from Ion Power®.

Purification of CNTs: preparation of oxidized CNTs

Two hundred milligrams of as-received MWCNTs was transferred to a round-bottomed flask containing the mixture of sulfuric acid and nitric acid (150 mL, volume ratio 3:1) and heated at 70 °C under continued stirring for 8 h. The reaction mixture was then cooled to room temperature and filtered. Afterward, the residual acid was removed by washing several times with distilled water until the pH of the filtrate was neutral. The pretreated MWCNTs were then dried in a hot air oven overnight at 60 °C. The obtained black solid is finally called Ox-CNTs. This later was used to prepare doped CNTs.

Heteroatom doping of CNTs

Heteroatom doping was carried out by thermal annealing as reported in the literature [23]. Preweighted Ox-CNTs were dispersed in 20 mL of distilled water using an ultrasonic bath. Thio-urea was added to this Ox-CNTs dispersion (the weight ratio of Ox-CNTs and thio-urea was maintained as 1:15, respectively), and the mixture was sonicated for 2 h and kept under mechanical stirring at room temperature for 24 h. The solvent was then evaporated via a hot plate. The obtained solid powders were finely grinded with a mortar and pestle. The gray solid was transferred into a silica boat and kept in a tubular furnace. Nitrogen gas was flowed through the tubular furnace for 2 h to purge and maintain the inert atmosphere. Afterward, under continues N_2 flow, the furnace was gradually heated to 800 °C and held for 2 h before cooling the furnace at room temperature. The obtained NS-Ox-CNTs sample was collected and preserved in airtight vials for further experiments.

Physicochemical characterizations

All studied samples were characterized via transmission electron microscopy (TEM), X-ray photoelectron spectroscopy (XPS), thermogravimetric analysis (TGA), Raman spectroscopy and elemental analysis. The measurement method for each device is described in below.

The TEM observations were carried out on a JEOL ARM 200F-Cold FEG operating at 80 kV. The samples were dispersed in ethanol, and a drop of the dispersion was deposited on a holey carbon-supported copper grid (200 mesh size) for analysis.

XPS spectra were collected on a Kratos Axis Ultra (Kratos Analytical, UK) spectrometer equipped with a monochromatic Al Kα (1486.6 eV). All spectra were recorded at a 90° takeoff angle. The high-resolution regions were acquired with 0.1 eV step and 20 eV pass energy (instrumental resolution better than 0.5 eV). Curve fitting was performed using a combined Gaussian and Lorentzian line profile after Shirley's background subtraction by Casa XPS software.

Thermogravimetric analysis (TGA-DTG) was performed with a Setaram Setsys evolution 1750 by using dry air as the carrier gas. Temperature ramp of 5 °C.min^{-1} from room temperature to 900 °C was used during the measurement.

Micro-Raman spectroscopy was carried out with a Jobin Yvon LabRAM HR800 equipped with a CCD detector, cooled at -70 °C. A 633 nm laser wavelength was used as the incident beam focused on the sample with microscope through a wide length × 50 objective. For each sample, at least 3 spectra were recorded from different area on the sample. For each spectrum, a background was subtracted and the maximum intensity of the D and the G bands were used to

calculate the D intensity over the G intensity ratio, I_D/I_G.

The elemental analysis of C, H, N, S was carried out by X-ray fluorescence by means of a Thermo Scientific Flash 2000 controlled by the Eager Xperience software.

Electrochemical characterization

The ORR activity of the prepared carbon catalysts was evaluated using cyclic voltammetry (CV) and linear sweep voltammetry (LSV) methods controlled by an electrochemical workstation [24]. All the experiments were performed in a three-electrode glass cell containing 1 M NaOH equipped with Hg/HgO reference electrode and Pt counter electrode. Glassy carbon (GC) with 5 mm of diameter is used to prepare the working electrode. GC was polished to obtain mirror shining surface prior to the catalyst ink deposition. For the all studied catalysts, the catalyst ink (1 mg.mL^{-1}) was prepared by dispersing the catalyst in a water ethanol mixture (volume ratio of 3:1) with 7.5wt. % of Nafion ionomer. This mixture was treated in an ultrasonic bath for 20 min to achieve greater homogeneity. From this ink, 4 aliquots of 10 µL were successively dropped and dried on GC surface for reaching a mass loading of 200 µg.cm^{-2}. After drying properly, GC was fixed to the rotating shaft and inserted in the electrochemical cell. The NaOH electrolyte was first saturated with nitrogen for recording the cyclic voltammogramm reference between the potentials 0.2 to -0.6 V vs Hg/Hgo (1 M NaOH). Then the solution was saturated with oxygen and CV curves were recorded at the same range of potentials. Moreover, LSV curves were recorded on the rotating disk electrode (RDE) by varying the rotating speed from 400 to 2500 rpm under a same potential range. For comparison, Pt/C (40 wt.%) was also tested under similar conditions.

At first approximation, electron transfer number (n) was estimated from LSV curves by applying Koutecký–Levich (K-L) equations in below [24].

$$i_d = B\omega^{-\frac{1}{2}} \quad (1)$$

$$B = 0.62nFC_{O2}D_{O_2}^{\frac{2}{3}}\vartheta^{-\frac{1}{2}} \quad (2)$$

ω is the rotation speed, n is the electron transfer number, F is the Faraday constant, D_{O_2} is the diffusion coefficient of oxygen (1.64 × 10^{-5} cm^2 s^{-1} in 1 M NaOH), C_{O_2} is the concentration of oxygen (8.4 × 10^{-7} mol cm^{-3} in 1 M NaOH), and ν is the kinematic viscosity (0.011 cm^2 s^{-1}).

Results and discussion

Oxidation/purification of CNTs

As-received CNT samples generally contain metallic impurities resulting from synthesis conditions for growing CNTs. Although these metallic impurities within CNTs are supposed to be inactive for ORR activity, their presence often leads to misinterpretation of the data as they can contribute to CNT properties such as surface area, density and conductivity. Then, it is important to remove these impurities from the CNT samples before measuring their electrochemical response. Since pristine CNTs are inert and electrically neutral, strong acids like H_2SO_4 and HNO_3 are usually used to induce their activation. Figure 1 shows TEM images of MWCNTs before (Figs. 1a and 1c) and after oxidation (Figs. 1b and 1d) at different magnifications. It can be seen that the tubular structure of CNTs is not affected by the oxidation. Further, from the low-magnification TEM images, the dark particles (higher electronic density than carbon) being the metallic impurities are present in the pristine MWCNTs (see yellow circles on

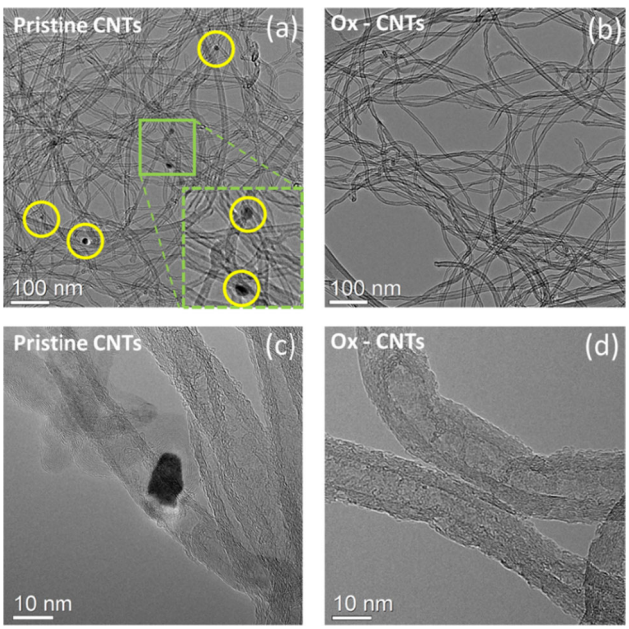

Figure 1 TEM images of **a**,**c** pristine CNTs and **b**,**d** Ox-CNTs at different magnifications.

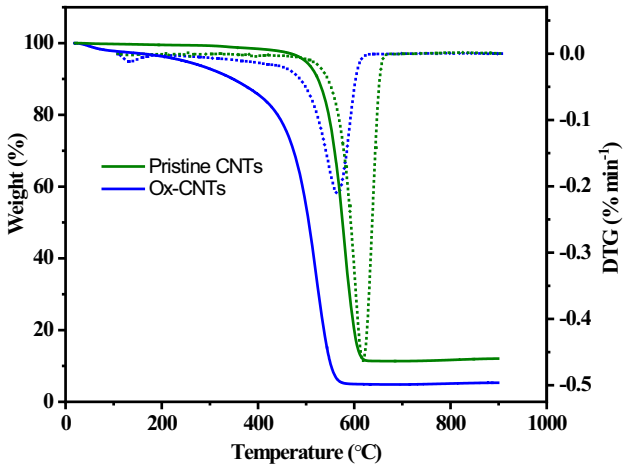

Figure 2 Thermogravimetric analysis of pristine CNTs and Ox-CNTs.

Fig. 1a) but not detectable after the oxidation by TEM because of their low content (cf. TGA analysis, Fig. 2).

Thermal degradation of MWCNTs under air by TGA allows i) to analyze the thermal stability of the MWCNTs, their combustion temperature being downshifted in the case of a weaker resistance to oxidation, and ii) to quantify the residual metal-based impurities coming from the catalysts used for the MWCNT growth. Results from TGA (Fig. 2) show that after the acidic treatment thermal, stability of Ox-CNTs is reduced since the combustion temperature is downshifted of 40 °C from 620 °C for pristine CNTs to 580 °C for Ox-CNTs. Moreover, the residual mass of the metallic impurities oxidized after TGA in Ox-CNTs is decreased from 11% (raw MWCNTs) down to 5% after the oxidation treatment. The content of the (non-oxidized) metal-based impurities in Ox-CNTs, which was not removed probably because they are non-accessible to the oxidative reagents, is estimated to be around 3 wt.% (cf. Supporting Information, section I).

XPS results show that the treated samples (Ox-CNTs) contain around 8% of oxygen atoms while pristine CNTs show only around 1% of oxygen (Supporting Information, Table S1 and Figure S1, Sect. 2) in agreement with an efficient oxidation occurrence by the applied acid-based treatment. Deconvoluted C 1 s and O 1 s signals of Ox-CNTs (Fig. 3) reveal the presence of carbonyl, hydroxyl and carbonyl functional groups (C = O, C–OH, COOH) [25, 26]. The used acid-based method has the advantage to both clean and purify the CNTs and induce an efficient oxidation of the CNTs in a one-pot process.

Heteroatom-doped CNTs

N-doped and NS-co-doped samples were prepared with melamine and thio-urea, respectively: melamine as unique nitrogen source and thio-urea as both nitrogen and sulfur source as depicted in Scheme 1. In order to study the impact of the pretreatment on MWCNTs, N-doped and NS-co-doped samples were prepared with oxidized MWCNTs (Ox-CNTs) and as-received MWCNTs (CNTs). The obtained samples were named N-CNTs and NS-CNTs for the pristine MWCNTs doped with melamine and thio-urea, respectively. The samples N-Ox-CNTs and NS-Ox-CNTs were named for the oxidized MWCNTs (Ox-CNTs) doped with melamine and thio-urea, respectively. In addition, the doping method remains the same for the both Ox-CNTs and pristine CNTs and the both sources as precursors.

Morphological characterization of heteroatom-doped CNTs

Figure 4 shows the TEM images for N-Ox-CNTs and NS-Ox-CNTs. It has to be noted that at high magnification, introduction of defects in the MWCNT walls is clearly noticed for N-Ox-CNTs and NS-Ox-CNTs (see yellow circles on Figs. 4c and 4d) in agreement with occurrence of the expecting covalent functionalization and grafting of oxygen-containing groups by oxidation and their doping since both chemical modifications are expected to damage the MWCNT walls. In general, the defects present in carbon nanomaterials are favorable for the ORR; for example, electronic state of the material is extremely improved at the topological defects [27]. It is established that the active sites for ORR in carbon materials are induced by the defect sites; further, the electronic state near the fermi level of MWCNTs can be altered by the crystal strain which can be induced through edges or basal plane defects. Therefore, the defects at the surface of MWCNTs and its engineering play a vital role toward the ORR properties of heteroatom-doped CNTs.

Raman spectroscopy is a powerful and widely used technique for chemically modified CNTs since it allows to evidence CNT damaging upon covalent functionalization. The G band found around 1575 cm^{-1} characterizes sp^2 carbon of crystalline

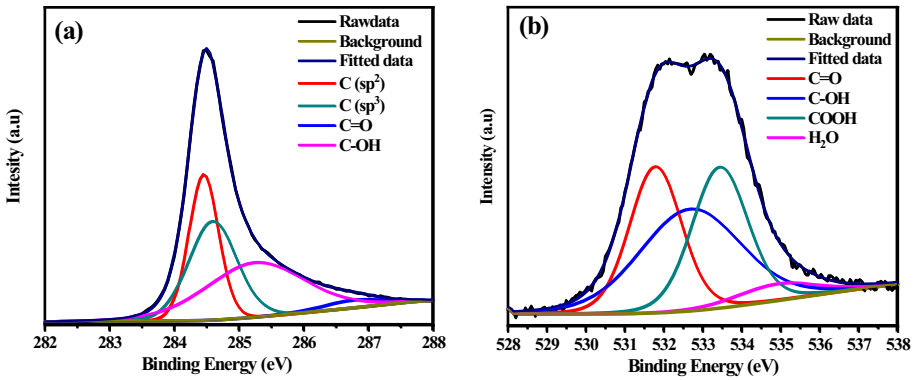

Figure 3 Deconvoluted XPS spectra of **a** C 1 s and and **b** O 1 s for Ox-CNTs.

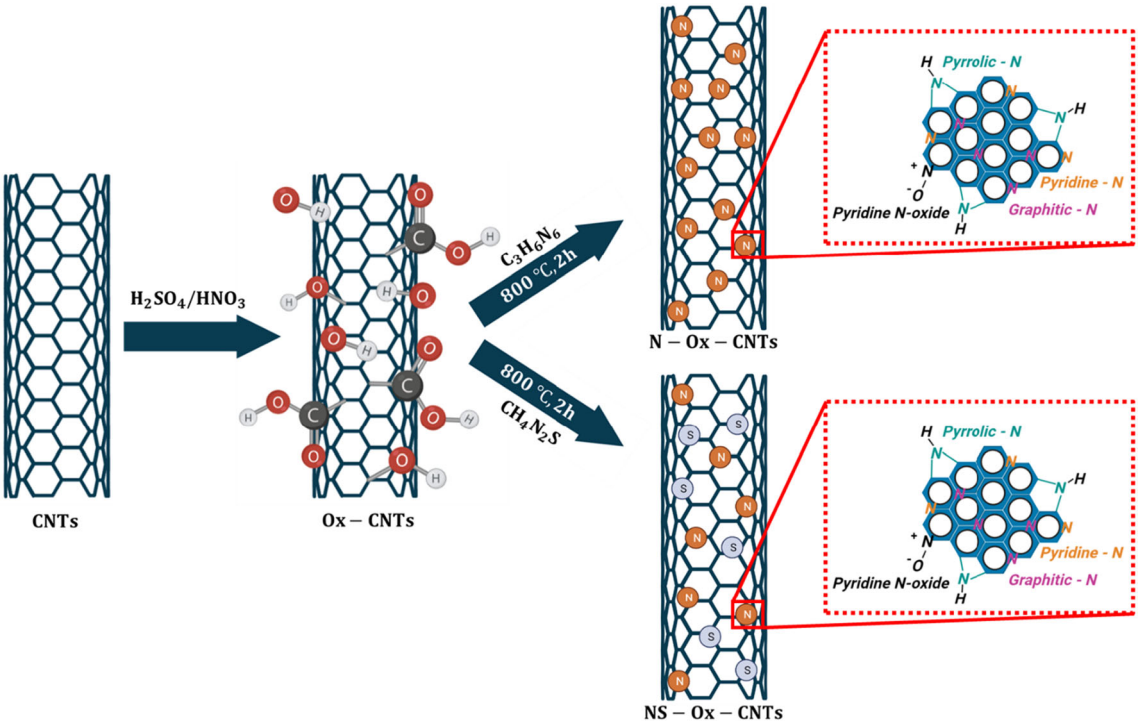

Scheme 1. Schematic representation of oxidation and subsequent heteroatom doping methods.

graphite, in particular in-plane vibration of sp^2-bonded carbon network [25]. The D band around 1320 cm^{-1} appears in a defected or disordered crystalline graphite. The ratio between the intensities of the D and G bands (I_D/I_G) is commonly used to quantify the disorder or introduction of defects in the sp^2 honeycomb structure. Figure 5 shows typical Raman spectra of pristine CNTs, Ox-CNTs, N-Ox-CNTs and NS-Ox-CNTs. The mean I_D/I_G ratio of the pristine MWCNT sample is 1.96 (± 0.07). After oxidation and subsequent doping, as expected, I_D/I_G has significantly increased up to 2.27 (± 0.01), 2.43 (± 0.09) and 2.63 (± 0.07). I_D/I_G evolves as follows: I_D/I_G (CNTs) < I_D/I_G (Ox-CNTs) < I_D/I_G (N-Ox-CNTs) < I_D/I_G (NS-Ox-CNTs), in agreement with introduction of defects under the form of oxygen-containing groups grafted to the CNT walls by acid oxidation and further introduction of N or N/S within the CNT framework by doping.

Elemental analysis of heteroatom-doped CNTs

According to the literature, the amount of the doped element and its precise configuration can have a great of influence on ORR activity. Table 1 summarizes the amount of four chemical elements (C, H, N and S)

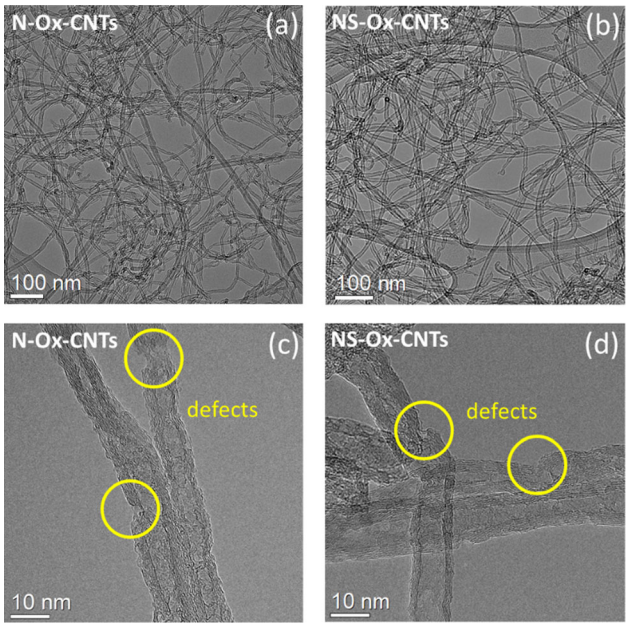

Figure 4 TEM images for **a**,**c** N-OX-CNTs **b**,**d** NS-Ox-CNTs.

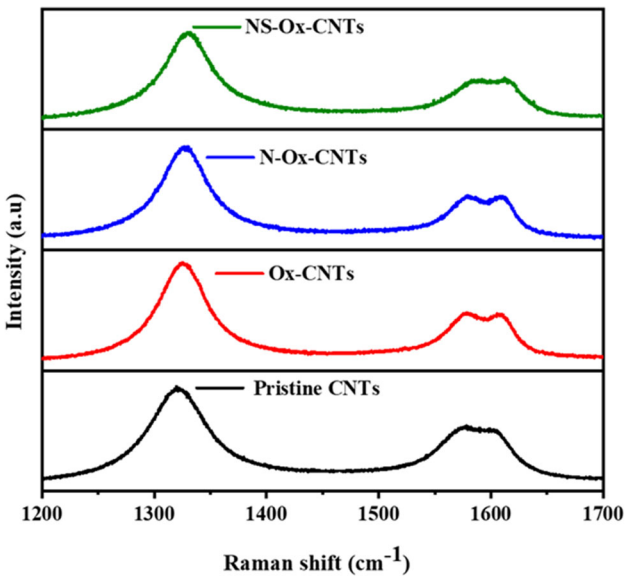

Figure 5 Raman spectra for pristine CNTs and functionalized CNTs.

contained within the all carbon samples studied in this work from elemental analysis. It is observed that doping occurs whatever the initial state of CNTs. However, the rate of doping is more than doubled when oxidized CNTs were used. This fact can be explained by defects introduced during the acid treatment leading to improvement of MWCNT chemical reactivity.

Table 1 Elemental analysis of the studied samples by X-ray fluorescence

Sample	C (%)	H (%)	N (%)	S (%)
Pristine CNTs	87.7	0.31	–	–
Ox-CNTs	78.7	0.66	–	–
N-CNTs	86.8	–	1.06	–
N-Ox-CNTs	91.02	–	2.84	–
NS-CNTs	83.05	0.25	1.0	0.24
NS-Ox-CNTs	87.05	0.33	2.2	0.93

As the Ox-CNTs doped materials appear to be more interesting than the untreated CNTs, further analysis was done for a better understanding of these prepared samples. For instance, Figures S2 and S3 show the XPS survey spectra of N-Ox-CNTs and NS-Ox-CNTs, the presence of N (at around 400 eV) and N,S (at around 400, 162 eV, respectively) is identified in the former and latter, respectively. Further deconvolution of N 1 s spectra of N-Ox-CNTs and NS-Ox-CNTs is shown in Figs. 6a and b which clearly highlights the four types of N environments at around 400 eV such as (i) pyridinic nitrogen, (ii) pyrolic nitrogen, (iii) graphitic nitrogen and (iv) oxide nitrogen. It is well known that the chemical states/configurations of N affect the ORR activity in different ways. Nitrogen types (i) and (iii) have been reported to be more active for ORR while nitrogen types (ii) and (iv) are less pronounced [28]. By deconvoluting N 1 s spectra of N-Ox-CNTs and NS-Ox-CNTs, the proportion of each nitrogen configuration is gathered in Table 2. The results reveal that nitrogen types (i) and (iii) are mainly represented in the doped samples (75% vs 90% for N-Ox-CNTs and NS-Ox-CNTs, respectively). The impact of this preferential nitrogen doping was further investigated by ORR measurements described below.

Contrary to the well-studied nitrogen configurations within doped carbon materials, the bonding configurations of S with C (Fig. 6c) in the NS-Ox-CNTs sample can be solely described as C-S 2p3/2 at 163.9 eV, 2p1/2 at 165.3 eV and C-SOx-C at 168.7 eV [29].

Electrochemical results

Cyclic voltammogramms were recorded in 1 M NaOH saturated nitrogen (black curves) or saturated

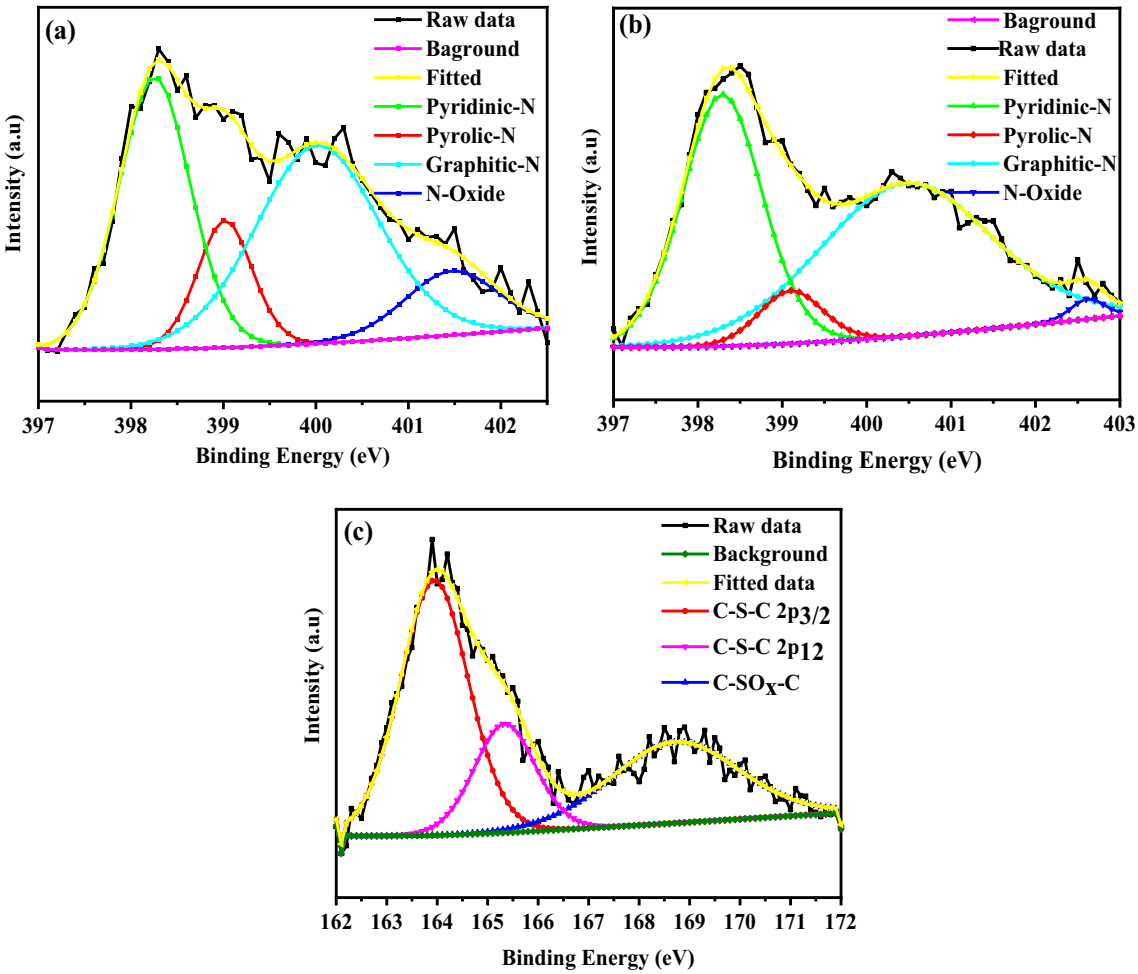

Figure 6 Decomposed XPS spectra of **a** N 1s in N-Ox-CNT, **b** N 1s of NS-Ox-CNT, **c** S 2p of NS-Ox-CNT.

Table 2 Quantification of different N functionalities in N-Ox-CNTs and NS-Ox-CNTs from XPS

Sample	Pyridinic-N (%)	Pyrolic-N (%)	Graphitic-N (%)	N-Oxide (%)
N-Ox-CNTs	42	16	33	9
NS-Ox-CNTs	48	8	42	2

oxygen (red curves) at 0 rpm (Fig. 7). The current density expressed here is calculated with the geometric area of the electrode (glassy carbon with a 5 mm diameter). The CV measurement with nitrogen is to do a blank and to check that nothing has occurred in the ORR area. Figure 7 (dark curves) shows well that no significant and characteristic peaks of reduced or oxidized species were observed for all studied samples. When the solution was saturated with oxygen, an ORR peak around 0.8 V is detected for all samples suggesting here that all studied samples have an ORR activity. Of course, this result is expected for doped samples and the rather high intensity of the ORR peak (near 0.7 – 0.8 mA.cm^{-2}) comforts us on the purpose of the modification. However, the presence of a small ORR peak (near 0.3 mA.cm^{-2}, at 0.78 V) observed on pristine CNTs can be rationalized by its (i) initial defect or disorder and (ii) metallic impurities.

Figure 8 shows the LSV (linear sweep voltammetry) curves of the measured samples at 1600 rpm. The curves allow to estimate the onset potential and the electron transfer number (n) during ORR. The ORR onset potential was measured at -0.1 mA.cm^{-2} [23], and it is considered to compare the activity of the synthesized catalysts with the one of Pt/C (Table 3).

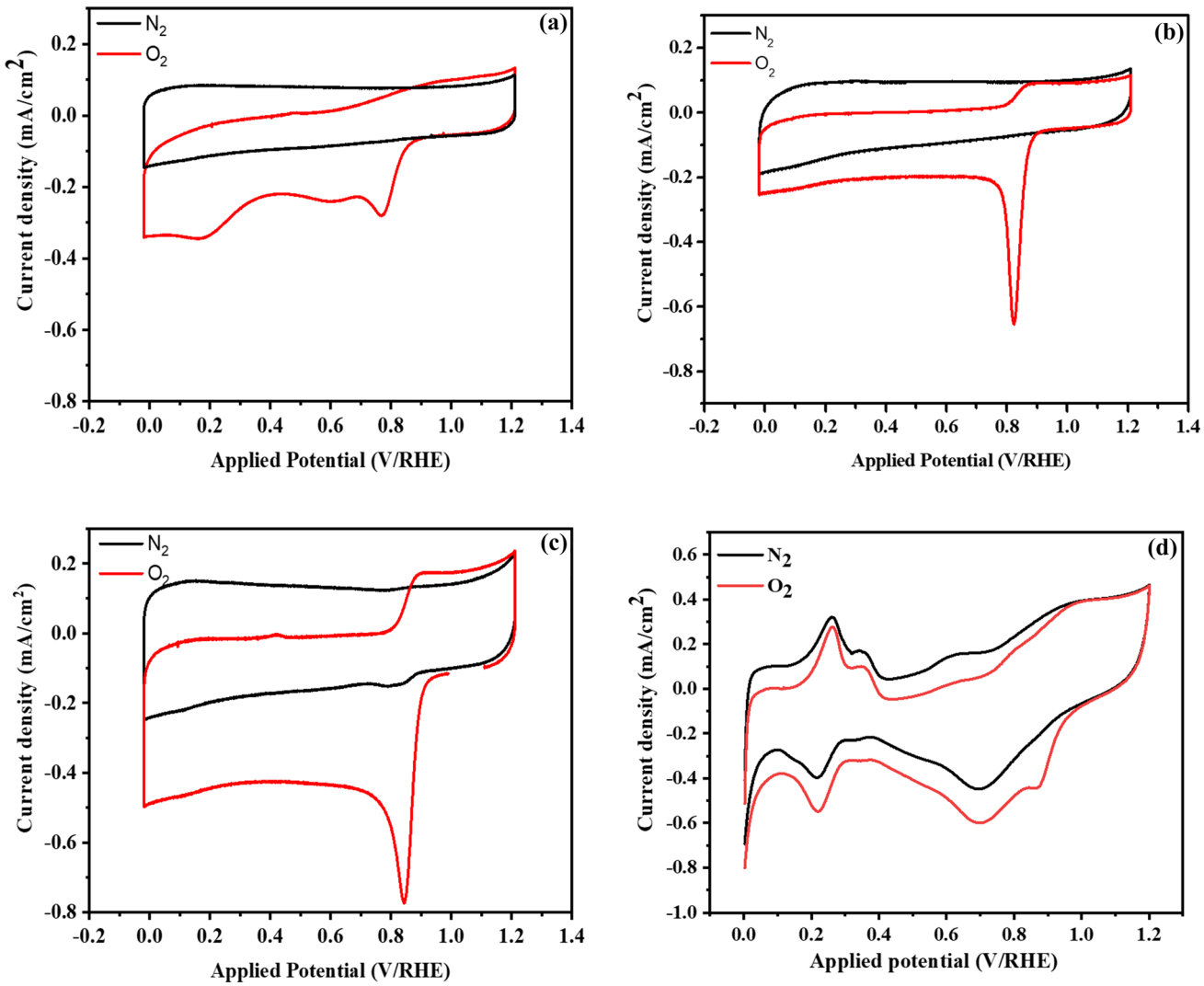

Figure 7 CV curves recorded for **a** pristine CNTs, **b** N-Ox-CNTs, **c** NS-Ox-CNTs and **d** Pt/C in N_2 and O_2 saturated 1 M NaOH.

Table 3 Electrochemical characteristics of heteroatom-doped CNTs compared with pristine CNTs and Pt/C

Samples	Over potential (V) @ 0.1 mA/cm^2	Limiting current density @0.4 V (mA/cm2)	Half-wave potential $E_{1/2}$ (V)	Electron transfer number (n)	ECSA (cm^2)
Pristine CNTs	0.83	1.2	0.74	2	0.87
N-CNTs	0.86	2.3	0.82	2.7	3.74
NS-CNTs	0.89	2.6	0.83	2.9	5.26
N-Ox-CNTs	0.92	2.8	0.84	3.70	5.63
NS-Ox-CNTs	0.95	3.3	0.88	3.95	9.06
Pt/C	0.98	3.3	0.88	4	–

As expected, the ORR onset potential for co-doped CNTs was shifted to higher potential compared to single atom-doped CNTs and pristine CNTs. It is interesting to note that N-Ox-CNT and NS-Ox-CNTs have shown significantly positive onset potential in comparison with their respective un-oxidized

versions (N-CNTs, NS-CNTs). The onset potential of NS-Ox-CNTs (@-0.1 mA/cm^2) is very much similar to that of Pt/C suggesting that oxidation and co-doping are an effective way to tailor the electrochemical properties of CNTs.

These results emphasize the beneficial effect of doping on CNTs and also highlight the synergy effect of co-doping on the electrochemical properties of CNTs. It is interesting to note that the oxidized CNTs have lower ORR activity compared to pristine CNTs due to the removal of any interfering metal atoms during the oxidation treatment.

Electron transfer number (n) during ORR can be estimated by varying the rotating rate of the rotating disk electrode (RDE). This number informs us on the possible way that ORR occurred within the catalyst. Theoretically, electron transfer number during ORR in an alkaline medium can be described via two mechanisms either (1) by 4 electrons pathway in which the oxygen molecule is directly reduced into 4 OH^- or (2) by 2 + 2 electrons pathway in which one hydrogen peroxide molecule in HO_2^- form acts as an intermediate species (see equations in bottom).

Since the indirect way generates intermediate species, the direct way with 4 electrons is generally preferred over the indirect way.

1. Direct way: $O_2 + 4e^- + 2H_2O = 4OH.^-$ ($E° = 0.401\ V_{SHE}$ at 298 K)
2. Indirect way: $O_2 + H_2O + 2e^- = HO_2^{-} + OH.^-$ ($E° = -0.065\ V_{SHE}$ at 298 K)
   $HO_2^- + 2e^- + H_2O = 3OH^-$ ($E°=0.867\ V_{SHE}$ at 298K)

However, there is not a lot of ways to determine n. The classical method is using a RDE and then extracting n from LSV curves by applying K-L equations. In the case of Pt/C for instance, LSV curves are first plotted at different rotating speed (ω in rpm) and under a same potential range (Fig. 9 (d). It is observed that the rotation speed increases the current density due to a better mass transport. At second, we have to plot the current density according to $\omega^{-1/2}$ as expressed in Eq. 1. At third, the number of transfer electron is calculated via the value of the slop of the K-L curve (Fig. 9(h)) and the Eq. 2.

In order to estimate the electron number of our prepared carbon samples, we have applied the same method as for Pt/C (Fig. 9 (a) to (f)). Due to the difference in material properties, the electrochemical response is not the same especially at low potential. As CNTs materials are porous, the retention time of species produced during ORR can be higher in comparison with smooth and flat electrode like Pt. For porous materials, the plateau at low potential (Fig. 9g) becomes a slop (Fig. 9a, c, e) at each applied speed and current depends on the chosen voltage [30]. In that case, there is not a unique n according to the range of potential. The electron transfer number (n) for all the prepared samples has been calculated at 0.4 V and is represented in Table 3. The maximum n values are obtained for undoped CNTs which are close to 2 indicating a dominant 2 + 2 electrons mechanism (indirect way)2e$^-$, while NS-OX-CNTs show a maximum n of 3.95 which is comparable to Pt/C (n = 4) being the sign that the ORR proceeds through 4e$^-$ process (direct way) on NS-OX-CNTs. Double-layer capacitance (C_{dl}) is estimated for the prepared samples by performing the CV in non-faradic region and at different voltage sweeps (20–100 mV s^{-1}) as shown in Figure S4 (Supporting Information, Sect. 4). Electrochemical active surface area (ECSA) is calculated from the double layer capacitance using the equation below [31].

$$ECSA = \frac{C_{dl}}{C_s} \tag{3}$$

where C_{dl} is the double-layer capacitance and C_s is the specific capacitance of the material which is reported as 0.040mF/cm^2[32, 33].

In addition, the ECSA for all heteroatom-doped CNTs is higher than that of the pristine CNTs. It is noteworthy that the ECSA is higher for N-Ox-CNTs

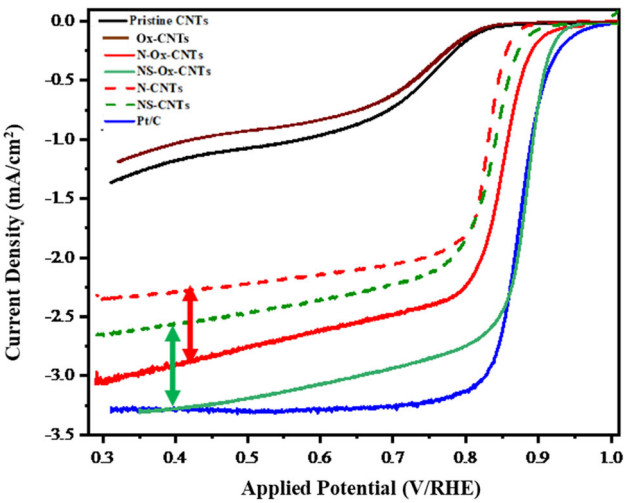

Figure 8 LSV data recorded in 1 M NaOH (O_2 saturated) for pristine CNTs, oxidized CNTs and heteroatom-doped CNTs compared with commercial Pt/C at 1600 rpm.

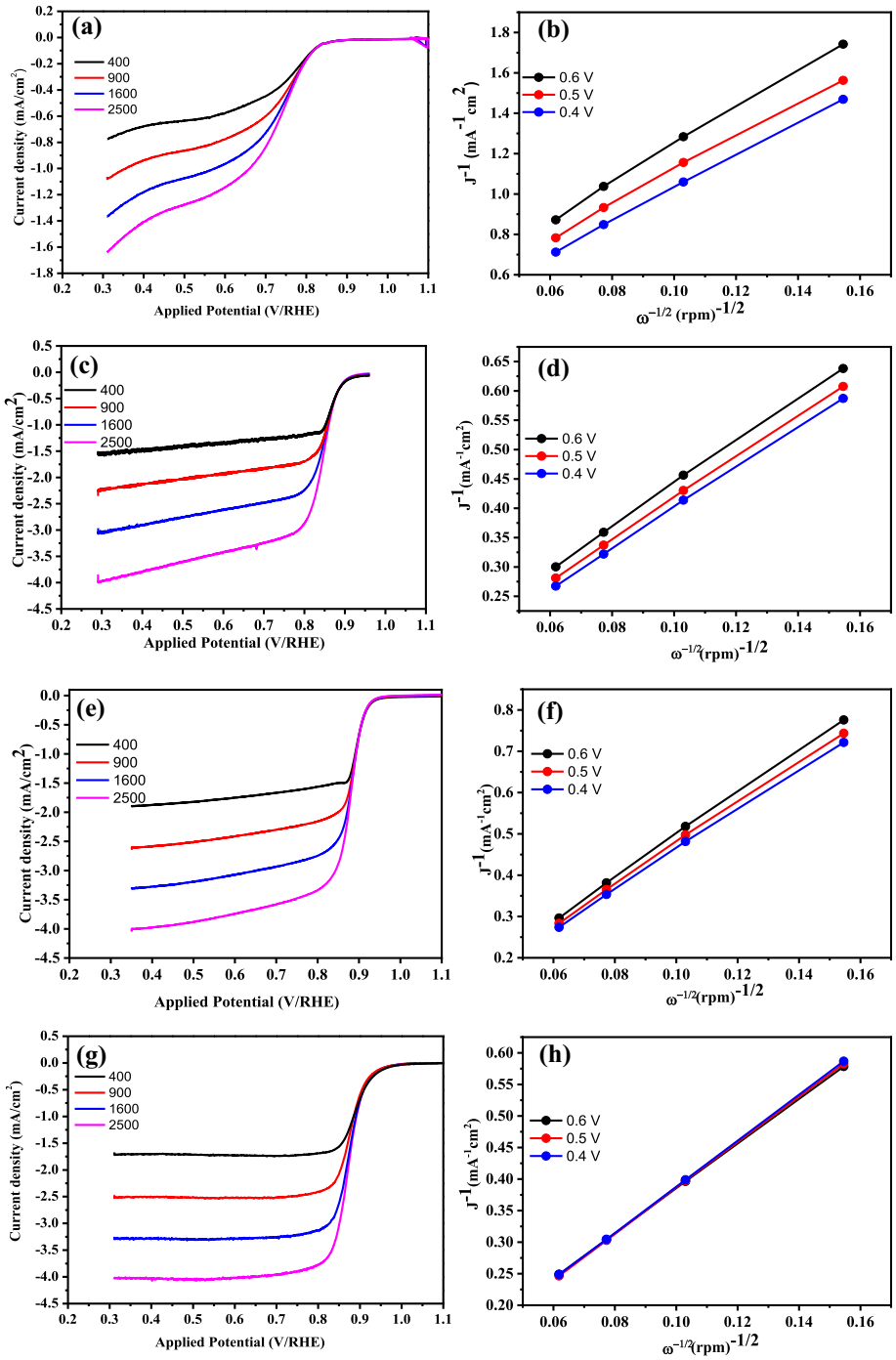

Figure 9 LSV curves and K-L plots for **a**,**b** pristine CNTs, **c**,**d** N-Ox-CNTs, **e**,**f** NS-Ox-CNTs, **g**,**h** Pt/C.

and NS-OX-CNTs compared to their analogues N-CNTs and NS-CNTs due to the greater number of accessible electrochemically active sites that are resulted from oxidation and successive heteroatom doping.

It is noteworthy that the result obtained for the prepared electrocatalysts is comparable with recently reported heteroatom-doped CNTs-based materials in terms of onset potential and electron transfer number and is listed in Table 4.

From the illustrated results, it is pointed out that (i) ORR occurred via a 2 + 2 electrons mechanism (by an indirect route) within undoped CNTs, (ii) both doped materials have a mixed of electron transfer mechanisms (4 electrons pathway direct route and 2 + 2 electrons mode) during ORR and (iii) the

Table 4 Comparison of results with the recently reported literature based in heteroatom-doped CNTs

Catalyst	Doped element (s) %	Source of heteroatom	ORR onset potential (V)	Electron transfer number	Ref
N-CNTs	N-8 at%	Poly(2-methyl-1-vinylimidazole)	− 0.05 vs Ag/AgCl	3.80	[34]
PN-CNTs	P—0.8 at%N—2.9 at%	Triphenylphosphine, ammonia	− 0.09 vs Ag/AgCl	3.67	[35]
N-CNTs	N-3–6%	Pyridine	− 0.22 Ag/AgCl	3.00	[36]
SN-CNTs	S – 0.18 at.% N – 3.02 at.%	Ammonia, sulfur powder	− 0.2 vs Ag/AgCl	3.40	[20]
N-CNTs	N-3.1 at%	Melamine	− 0.159 vs Ag/AgCl	3.30	[19]
N-UCNTs	N-6.65 at%	Melamine	− 0.08 vs Ag/AgCl	3.38	[37]
B – CNTs	B-2.24 at%	Triphenylborane	− 0.25 vs Ag/Agcl	2.50	[38]
N-Ox-CNTs	N-2.2%	Melamine	0.92 vs RHE (− 0.08 vs Ag/AgCl)	3.70	This work
NS-Ox-CNTs	N-2.2% S-0.93%	Thio-urea	0.95 vs RHE (− 0.05vs Ag/AgCl)	3.95	This work

number of transfer electron of NS-Ox-CNTs is comparable to the one of Pt/C at 0.4 V. Based on this observation, we can stand that co-doping is indeed a better strategy than single doping for improving ORR.

Conclusions

The goal of improving ORR activity of MWCNTs (CNTs) can be achieved by acid pretreatment and heteroatom doping (N-doping and NS-co-doping). This study reveals that the applied acid-based method is very efficient to remove unwanted impurities remaining in the pristine CNTs as well as to induce oxygen-containing functional groups within the MWCNT framework. As a consequence, the amount of doping element is increased when used pretreated CNTs. Melamine and thio-urea were compared as mono-source (N) and co-sources (NS) elements for doping. The comparison of N-doping and NS-co-doping highlights the synergy effect of two different heteroatoms over a unique heteroatom. In fact, N can promote density charge change, whereas S can promote spin density change. Moreover, a higher amount of pyridinic and graphitic nitrogen is measured when thio-urea is used for doping. The combination of N and S interaction and the rich proportion of pyridinic and graphitic functionalities within CNTs favor considerably ORR activity in terms of E_{ONSET} and the number of electron transfer (n). As a result, the electrochemical response of the prepared NS-Ox-CNTs sample is close to the commercial Pt/C. This encouraging result envisions AEMFC tests with this Pt-free catalyst at the cathode side and also the development of other metal-free catalysts.

Acknowledgments

The authors acknowledge support for LEMTA and IJL by the " IMPACT ULHyS, Universite de Lorraine Hydrogene Science et Technologie" project of the "Lorraine Universite d'Excellence" (Investissements d'avenir e ANR). This work was supported partly by the french PIA project « Lorraine Universite d'Excellence », reference ANR-15-IDEX-04-LUE. The authors would like to thank L. Aranda for his help for TGA experiment. We would like to thank the imaging core facility called "Microscopies, Microprobes and Metallography (3M)" (Institut Jean Lamour, IJL, Nancy, France) and J. Ghanbaja and Christine Gendarme for their valuable help. We thank Stéphanie Michel for the elemental analysis of the prepared samples. We would like to thank the platform "Optics and laser" (Institut Jean Lamour, IJL, Nancy, France). We would like to thank the vibrational spectroscopy platform called CC Optique Lasers "Spectroscopies et Microscopies des Interfaces" (Laboratory of Physical

Chemistry and Microbiology for Materials and the Environment, LCPME, Nancy, France) and A. Renard, Dr. M. Mallet (LCPME) for XPS analysis.

Declarations

Conflict of interest The authors declare no conflict of interest.

Supplementary Information: The online version contains supplementary material available at https://doi.org/10.1007/s10853-022-07653-3.

References

[1] Firouzjaie Horie Adabi, Mustain William E (2019) Catalytic Advantages, Challenges, and Priorities in Alkaline Membrane Fuel Cells. ACS Catalysis 10(1):225–234. https://doi.org/10.1021/acscatal.9b03892

[2] Raccichini R, Varzi A, Passerini S, Scrosati B (2015) The role of graphene for electrochemical energy storage. Nat Mater 14(3):271–279. https://doi.org/10.1038/nmat4170

[3] Bing Y, Liu H, Zhang L, Ghosh D, Zhang J (2010) Nanostructured Pt-alloy electrocatalysts for PEM fuel cell oxygen reduction reaction. Chem Soc Rev 39(6):2184–2202. https://doi.org/10.1039/b912552c

[4] Gutru R, Turtayeva Z, Feina Xu, Maranzana G, Vigolo B, Desforges A (2020) A comprehensive review on water management strategies and developments in anion exchange membrane fuel cells. Inter J Hydrogen Energy 45(38):19642–19663. https://doi.org/10.1016/j.ijhydene.2020.05.026

[5] Shao M, Chang Q, Dodelet J-P, Chenitz R (2016) Recent Advances in Electrocatalysts for Oxygen Reduction Reaction. Chem Rev 116(6):3594–3657. https://doi.org/10.1021/acs.chemrev.5b00462

[6] Rabis A, Rodriguez P, Schmidt TJ (2012) Electrocatalysis for Polymer Electrolyte Fuel Cells: Recent Achievements and Future Challenges. ACS Catal 2(5):864–890. https://doi.org/10.1021/cs3000864

[7] Akula S, Parthiban V, Peera SG, Singh BP, Dhakate SR, Sahu AK (2017) Simultaneous Co-Doping of Nitrogen and Fluorine into MWCNTs: An In-Situ Conversion to Graphene Like Sheets and Its Electro-Catalytic Activity toward Oxygen Reduction Reaction. J Electrochem Soc 164(6):F568–F576. https://doi.org/10.1149/2.0501706jes

[8] Woo J, Lim JS, Kim JH, Joo SH (2021) Heteroatom-doped carbon-based oxygen reduction electrocatalysts with tailored four-electron and two-electron selectivity. Chem Commun 57(60):7350–7361. https://doi.org/10.1039/D1CC02667D

[9] Yang K, Zaffran J, Yang B (2020) Fast prediction of oxygen reduction reaction activity on carbon nanotubes with a localized geometric descriptor. Phys Chem Chem Phys 22(2):890–895. https://doi.org/10.1039/C9CP04885E

[10] Zhang Y, Zhang J, Su DS (2014) Substitutional Doping of Carbon Nanotubes with Heteroatoms and Their Chemical Applications. Chemsuschem 7(5):1240–1250. https://doi.org/10.1002/cssc.201301166

[11] Shao Y, Jiang Z, Zhang Q, Guan J (2019) Progress in Nonmetal-Doped Graphene Electrocatalysts for the Oxygen Reduction Reaction. Chemsuschem 12(10):2133–2146. https://doi.org/10.1002/CSSC.201900060

[12] Daniel G, Mazzucato M, Brandiele R, De Lazzari L, Badocco D, Pastore P, Kosmala T, Granozzi G, Durante C (2021) Sulfur Doping versus Hierarchical Pore Structure: The Dominating Effect on the Fe-N-C Site Density, Activity, and Selectivity in Oxygen Reduction Reaction Electrocatalysis. ACS Appl. Mater. Interfaces 13(36):42693–42705. https://doi.org/10.1021/ACSAMI.1C09659

[13] Tavakol H, Keshavarzipour F (2016) A sulfur doped carbon nanotube as a potential catalyst for the oxygen reduction reaction. RSC Adv 6(67):63084–63090. https://doi.org/10.1039/c6ra11447d

[14] Li J-C, Hou P-X, Liu C (2017) Heteroatom-Doped Carbon Nanotube and Graphene-Based Electrocatalysts for Oxygen Reduction Reaction. Small 13(45):1702002. https://doi.org/10.1002/smll.201702002

[15] Peera SG, Koutavarapu R, Akula S, Asokan A, Moni P, Selvaraj M, Balamurugan J, Kim SO, Liu C, Sahu AK (2021) Carbon nanofibers as potential catalyst support for fuel cell cathodes: a review. Energy Fuels 35(15):11761–11799. https://doi.org/10.1021/ACS.ENER

GYFUELS.1C01439/ASSET/IMAGES/MEDIUM/EF1C01439_0017.GIF

[16] C. E. Nelson, C. H. Hakim, D. G. Ousterout, P. I. Thakore, E. A. Moreb, R. M. C. Rivera, S. Madhavan, X. Pan, F. A. Ran, W. X. Yan, A. Asokan, F. Zhang, D. Duan, and C. A. Gersbach, "In vivo genome editing improves muscle function in a mouse model of Duchenne muscular dystrophy," *Science (80-.).*, vol. 351, no. 6271, pp. 403–407, Jan. 2016, doi: https://doi.org/10.1126/science.aad5143.

[17] Zhu T-J, Chen X, Cao Y-Q, Zhao X-B (2009) Controllable Synthesis and Shape Evolution of PbTe Three-Dimensional Hierarchical Superstructures via an Alkaline Hydrothermal Method. J Phys Chem C 113(19):8085–8091. https://doi.org/10.1021/jp900452b

[18] Peera SG, Kwon H-J, Lee T G, Mohammed Hussain A (2020) Heteroatom- and metalloid-doped carbon catalysts for oxygen reduction reaction: a mini-review. Ionics 26(4):1563–1589. https://doi.org/10.1007/s11581-020-03473-0

[19] Rocha IM, Soares OSGP, Fernandes DM, Freire C, Figueiredo JL, Pereira MFR (2016) N-doped Carbon Nanotubes for the Oxygen Reduction Reaction in Alkaline Medium: Synergistic Relationship between Pyridinic and Quaternary Nitrogen. ChemistrySelect 1(10):2522–2530. https://doi.org/10.1002/slct.201600615

[20] Shi Q, Peng F, Liao S, Wang H, Yu H, Liu Z, Zhang B, Su D (2013) Sulfur and nitrogen co-doped carbon nanotubes for enhancing electrochemical oxygen reduction activity in acidic and alkaline media. J Mater Chem A 1(47):14853. https://doi.org/10.1039/c3ta12647a

[21] Zhao Y, Yang L, Chen S, Wang X, Ma Y, Wu Q, Jiang Y, Qian W, Hu Z (2013) Can Boron and Nitrogen Co-doping Improve Oxygen Reduction Reaction Activity of Carbon Nanotubes? J Am Chem Soc 135(4):1201–1204. https://doi.org/10.1021/ja310566z

[22] Peera S G, Liu Chao (2022) Unconventional and scalable synthesis of non-precious metal electrocatalysts for practical proton exchange membrane and alkaline fuel cells: A solid-state co-ordination synthesis approach. Coordination Chem Rev 463:214554. https://doi.org/10.1016/j.ccr.2022.214554

[23] Peera SG, Arunchander A, Sahu AK (2016) Cumulative effect of transition metals on nitrogen and fluorine co-doped graphite nanofibers: an efficient and highly durable non-precious metal catalyst for the oxygen reduction reaction. Nanoscale 8(30):14650–14664. https://doi.org/10.1039/C6NR02263D

[24] Poux T, Napolskiy FS, Dintzer T, Kéranguéven G, Istomin SY, Tsirlina GA, Antipov EV, Savinova ER (2012) Dual role of carbon in the catalytic layers of perovskite/carbon composites for the electrocatalytic oxygen reduction reaction. Catal Today 189(1):83–92. https://doi.org/10.1016/j.cattod.2012.04.046

[25] Pacheco FG, Cotta AAC, Gorgulho HF, Santos AP, Macedo WAA, Furtado CA (2015) Comparative temporal analysis of multiwalled carbon nanotube oxidation reactions: Evaluating chemical modifications on true nanotube surface. Appl Surf Sci 357:1015–1023. https://doi.org/10.1016/j.apsusc.2015.09.054

[26] Rambabu G, Nagaraju N, Bhat SD (2016) Functionalized fullerene embedded in Nafion matrix: A modified composite membrane electrolyte for direct methanol fuel cells. Chem Eng J 306:43–52. https://doi.org/10.1016/j.cej.2016.07.032

[27] Tang C, Zhang Q (2017) Nanocarbon for Oxygen Reduction Electrocatalysis: Dopants, Edges, and Defects. Adv Mater 29(13):1604103. https://doi.org/10.1002/ADMA.201604103

[28] Kim H, Lee K, Woo SI, Jung Y (2011) On the mechanism of enhanced oxygen reduction reaction in nitrogen-doped graphene nanoribbons. Phys Chem Chem Phys 13(39):17505. https://doi.org/10.1039/c1cp21665a

[29] Li C, Xie B, Chen J, He J, He Z (2017) Enhancement of nitrogen and sulfur co-doping on the electrocatalytic properties of carbon nanotubes for VO 2+ /VO 2 + redox reaction. RSC Adv 7(22):13184–13190. https://doi.org/10.1039/C6RA27734A

[30] Faisal SN, Haque E, Noorbehesht N, Zhang W, Harris AT, Church TL, Minett AI (2017) Pyridinic and graphitic nitrogen-rich graphene for high-performance supercapacitors and metal-free bifunctional electrocatalysts for ORR and OER. RSC Adv 7(29):17950–17958. https://doi.org/10.1039/C7RA01355H

[31] Suryanto BHR, Zhao C (2016) Surface-oxidized carbon black as a catalyst for the water oxidation and alcohol oxidation reactions. Chem Commun 52(38):6439–6442. https://doi.org/10.1039/c6cc01319h

[32] Bisen OY, Atif S, Mallya A, Nanda KK (2022) Self-Assembled TMD Nanoparticles on N-Doped Carbon Nanostructures for Oxygen Reduction Reaction and Electrochemical Oxygen Sensing Thereof. ACS Appl Mater Interfaces 14(4):5134–5148. https://doi.org/10.1021/acsami.1c11300

[33] McCrory CCL, Jung S, Peters JC, Jaramillo TF (2013) Benchmarking heterogeneous electrocatalysts for the oxygen evolution reaction. J Am Chem Soc 135(45):16977–16987. https://doi.org/10.1021/ja407115p

[34] Venkateswara Rao C, Ishikawa Y (2012) Activity, selectivity, and anion-exchange membrane fuel cell performance of virtually metal-free nitrogen-doped carbon nanotube electrodes for oxygen reduction reaction. J Phys Chem C 116(6):4340–4346. https://doi.org/10.1021/JP210840A/SUPPL_FILE/JP210840A_SI_001.PDF

[35] Yu D, Xue Y, Dai L (2012) Vertically Aligned Carbon Nanotube Arrays Co-doped with Phosphorus and Nitrogen as Efficient Metal-Free Electrocatalysts for Oxygen Reduction. J Phys Chem Lett 3(19):2863–2870. https://doi.org/10.1021/jz3011833

[36] Sharifi T, Hu G, Jia X, Wågberg T (2012) Formation of Active Sites for Oxygen Reduction Reactions by Transformation of Nitrogen Functionalities in Nitrogen-Doped Carbon Nanotubes. ACS Nano 6(10):8904–8912. https://doi.org/10.1021/nn302906r

[37] Chen L, Zhou H, Wei S, Chen Z, Huang Z, Huang Z, Zhang C, Kuang Y (2015) Facile synthesis of nitrogen-doped unzipped carbon nanotubes and their electrochemical properties. RSC Adv 5(11):8175–8181. https://doi.org/10.1039/c4ra15008b

[38] Yang L, Jiang S, Zhao Y, Zhu L, Chen S, Wang X, Wu Q, Ma J, Ma Y, Hu Z (2011) Boron-Doped Carbon Nanotubes as Metal-Free Electrocatalysts for the Oxygen Reduction Reaction. Angew Chemie Int Ed 50(31):7132–7135. https://doi.org/10.1002/anie.201101287